TIME-SPACE MULTISCALE ANALYSIS BY USE OF TENSOR PRODUCT WAVELETS AND ITS APPLICATION TO HYDROLOGY AND GRACE DATA

H. NUTZ AND K. WOLF

Geomathematics Group, Department of Mathematics, University of Kaiserslautern, P.O. Box 3049, 67653 Kaiserslautern, Germany (hnutz@rhrk.uni-kl.de, kerstin-wlf@gmx.de)

Received: July 11, 2007; Revised: March 31, 2008; Accepted: April 8, 2008

ABSTRACT

This paper presents a wavelet analysis of temporal and spatial variations of the Earth's gravitational potential based on tensor product wavelets. The time-space wavelet concept is realized by combining Legendre wavelets for the time domain and spherical wavelets for the space domain. In consequence, a multiresolution analysis for both temporal and spatial resolution is formulated within a unified concept. The method is then numerically realized by using first synthetically generated data and finally two real data sets.

Key words: multiresolution analysis, spherical wavelets, Legendre wavelets, time-space multiresolution analysis

1. INTRODUCTION

The huge amount of data provided by the satellite gravity mission GRACE (Gravity Recovery And Climate Experience) *Tapley et al. (2004)* allows for the first time to quantify both temporal and spatial variations of the Earth's gravity field caused by mass transport and mass distribution *Wahr et al. (2004)*. In order to model spatial variations of the Earth's gravitational potential the multiresolution technique using spherical wavelets has been developed by the Geomathematics Group of the TU Kaiserslautern in recent years, see *Freeden et al. (1998)* and the references therein. The wavelets which are radial basis functions on the sphere based on spherical harmonics are defined in frequency domain which allows to base the computations directly on the available data. The wavelets serve as band pass filters of Fourier coefficients where the band-width depends on a scale parameter. The higher the scale the higher is the degree of the Fourier coefficients which are filtered out. This is the so-called zooming-in property of the wavelet analysis because with increasing scale finer details are identified. The lower scales represent the coarse parts of the signal whereas the higher scales represent the smaller structures. The advantage of the multiresolution in comparison to the classical approach with spherical harmonics arises from the space localizing property of the used

basis functions in contrast to the localization in the frequency domain using spherical harmonics. Thus, the wavelets are an appropriate tool for the analysis of regional characteristics of a signal in $\mathcal{L}^2(\Omega)$.

First results concerning the temporal and spatial analysis of satellite data based on spherical wavelets have been published in *Fengler et al. (2007)* but in the approach presented there the wavelet analysis is only performed in the spatial domain. In order to transfer the classical method of tensor product wavelets as introduced in *Louis et al. (1998)* and *Maaß and Stark (1994)* we use the Legendre wavelets presented in *Beth and Viell (1998)* and *Viell (1998)* which are the counterparts of the spherical wavelets in the space $\mathcal{L}^2([-1,1])$. A first approach of the combined temporal and spatial wavelet analysis has been performed in *Freeden (1999)* and *Michel (1999)* for scalar fields and *Maier (2002)* for vector fields concerning geomagnetism. Starting from some ideas of these theses we are also able to establish pure and hybrid wavelets to measure both temporal and spatial changes in the gravity signal. But in contrast to the theory explained there we use one single scale and, therefore, arrive at a unified temporal and spatial multiresolution analysis of $\mathcal{L}^2([-1,1]\times\Omega)$.

The layout of the paper is as follows. We start introducing some important notation and symbols (Section 2). In order to explain the wavelet concept we present a general multiresolution analysis and define the spherical and the Legendre wavelets as special cases in Section 3. The combined time-space multiresolution analysis for reconstructing a signal in the temporal and spatial domain is then discussed in Section 4. Section 5 shows one synthetic example and then some results computed with satellite data from GRACE, see *GRACE Mission*, and hydrological data from WGHM (WaterGAP Global Hydrology Model), see *Döll et al. (2003)*, are presented. In the last section we summarize our results.

2. PRELIMINARIES

In this section we briefly recapitulate some notation and symbols which will be important within this paper. Further information can be found in *Freeden et al. (1998)*, *Müller (1966)* and the references therein.

The letters $\mathbb{N}$, $\mathbb{N}_0$, $\mathbb{Z}$ and $\mathbb{R}$ denote the sets of positive integers, non-negative integers, integers and real numbers, respectively. Ω is the unit sphere and ξ, η represent elements of Ω. The space of all real, square-integrable functions F on Ω is called $\mathcal{L}^2(\Omega)$. $\mathcal{L}^2(\Omega)$ is a Hilbert space with the inner product given by

$$(F,G)_{\mathcal{L}^2(\Omega)} = \int_{\Omega} F(\xi)G(\xi)\,d\omega(\xi), \quad F,G\in\mathcal{L}^2(\Omega). \tag{1}$$

The space of all scalar spherical harmonics $Y_n:\Omega\to\mathbb{R}$ of degree n is of dimension $2n+1$ and the set of spherical harmonics $Y_{n,k}:\Omega\to\mathbb{R}$ of degree $n\in\mathbb{N}_0$ and order

$k = 1, ..., 2n + 1$ forms an orthonormal basis of $\mathcal{L}^2(\Omega)$. Thus F can be uniquely represented by a Fourier series in $\mathcal{L}^2(\Omega)$-sense

$$F = \sum_{n=0}^{\infty} \sum_{k=1}^{2n+1} F^{\wedge}(n,k) Y_{n,k} , \tag{2}$$

where $F^{\wedge}(n,k)$ are called Fourier coefficients.

Closely related to the spherical harmonics are the Legendre polynomials $P_n : [-1,1] \to \mathbb{R}$ of degree n, $n \in \mathbb{N}_0$. Considering the space $\mathcal{L}^2([-1,1])$ with scalar product $(F,G)_{\mathcal{L}^2([-1,1])} = \int_{-1}^{1} F(t) G(t) \mathrm{d}t$, $F, G \in \mathcal{L}^2([-1,1])$, the $\mathcal{L}^2([-1,1])$-orthonormal Legendre polynomials $P_n^* : [-1,1] \to \mathbb{R}$ given by $P_n^* = [(2n+1)/2]^{\frac{1}{2}} P_n$, $n \in \mathbb{N}_0$, form an orthonormal basis in $\mathcal{L}^2([-1,1])$. Therefore every $F \in \mathcal{L}^2([-1,1])$ can be described in a series of the form $F = \sum_{n=0}^{\infty} F^{\wedge}(n) P_n^*$, which is called the Legendre expansion with Legendre coefficients $F^{\wedge}(n)$. The relation between the Legendre polynomial of degree n and the spherical harmonics of degree n is given by the addition theorem $\sum_{k=1}^{2n+1} Y_{n,k}(\xi) Y_{n,k}(\eta) = [(2n+1)/4\pi] P_n(\xi \cdot \eta)$, $\xi, \eta \in \Omega$.

3. MULTIRESOLUTION ANALYSIS

For a better understanding of the combined time-space theory and in order to provide the necessary notation we present an overview of multiresolution analysis following *Freeden and Schneider (1998)* and the references therein. As a matter of fact most of the functions in geophysics and geodesy are of bounded energy and thus we conclude this section with a short introduction to the Hilbert spaces $\mathcal{L}^2([-1,1])$ and $\mathcal{L}^2(\Omega)$.

Let $\mathcal{H}$ be a real separable Hilbert space over a certain domain $\Sigma \subset \mathbb{R}^m$ with inner product $(\cdot,\cdot)_{\mathcal{H}}$. Furthermore let $\{U_n^*\}_{n \in \mathbb{N}_0}$ be an orthonormal system which is complete in $(\mathcal{H}, (\cdot,\cdot)_{\mathcal{H}})$. Then we define the $\mathcal{H}$-product kernel $\Gamma : \Sigma \times \Sigma \to \mathbb{R}$ by

$$\Gamma(x,y) = \sum_{n=0}^{\infty} \Gamma^{\wedge}(n) U_n^*(x) U_n^*(y), \qquad x, y \in \Sigma , \tag{3}$$

with symbol $\{\Gamma^{\wedge}(n)\}_{n \in \mathbb{N}_0}$. A kernel function $\Gamma : \Sigma \times \Sigma \to \mathbb{R}$ is called $\mathcal{H}$-admissible if the following two conditions are satisfied:

$$\sum_{n=0}^{\infty} \left(\Gamma^{\wedge}(n)\right)^2 < \infty\,, \tag{4a}$$

$$\sum_{n=0}^{\infty} \left(\Gamma^{\wedge}(n) U_n^*(x)\right)^2 < \infty\,, \quad \forall x \in \Sigma\,. \tag{4b}$$

The admissibility conditions guarantee that the functions $\Gamma(x,\cdot): \Sigma \to \mathbb{R}$ and $\Gamma(\cdot,x): \Sigma \to \mathbb{R}$, $x \in \Sigma$ fixed, are elements of $\mathcal{H}$. Furthermore, they also ensure that the convolution of an admissible kernel function Γ and a function $F \in \mathcal{H}$ is again in $\mathcal{H}$, where the convolution is defined as follows: let $\Gamma: \Sigma \times \Sigma \to \mathbb{R}$ be an $\mathcal{H}$-admissible kernel function and $F \in \mathcal{H}$. The convolution of Γ against F is defined by

$$(\Gamma * F)(x) = \int_{\Sigma} F(y)\Gamma(x,y)\,dy = \sum_{n=0}^{\infty} \Gamma^{\wedge}(n) F^{\wedge}(n) U_n^*(x)\,. \tag{5}$$

Next we introduce the generating symbol of an $\mathcal{H}$-scaling function which finally leads to the definition of the $\mathcal{H}$-scaling function. $(\Phi_0)^{\wedge}(n)$ be the symbol of an $\mathcal{H}$-admissible kernel function which additionally satisfies the following two conditions:

$$(\Phi_0)^{\wedge}(0) = 1\,, \tag{6a}$$

$$\text{if } n > k \text{ then } (\Phi_0)^{\wedge}(n) \le (\Phi_0)^{\wedge}(k)\,. \tag{6b}$$

Then $(\Phi_0)^{\wedge}(n)$ is called the generating symbol of the mother $\mathcal{H}$-scaling function given by

$$\Phi_0(x,y) = \sum_{n=0}^{\infty} (\Phi_0)^{\wedge}(n) U_n^*(x) U_n^*(y)\,, \quad x,y \in \Sigma\,. \tag{7}$$

Since we are interested in the dilated versions of the mother $\mathcal{H}$-scaling function, we have to extend the definition of the generating symbol in the following way: let $\left\{(\Phi_J)^{\wedge}(n)\right\}_{n \in \mathbb{N}_0}$, $J \in \mathbb{Z}$, be an $\mathcal{H}$-admissible symbol satisfying in addition the following properties:

$$\lim_{J \to \infty} (\Phi_J)^{\wedge}(n) = 1\,, \quad n \in \mathbb{N}\,, \tag{8a}$$

$$(\Phi_J)^{\wedge}(n) \ge (\Phi_{J-1})^{\wedge}(n)\,, \quad J \in \mathbb{Z}\,, \quad n \in \mathbb{N}\,, \tag{8b}$$

$$\lim_{J \to -\infty} \left(\Phi_J\right)^{\wedge}(n) = 0, \quad n \in \mathbb{N}, \tag{8c}$$

$$\left(\Phi_J\right)^{\wedge}(0) = 1, \quad J \in \mathbb{Z}. \tag{8d}$$

Then $\left\{\left(\Phi_J\right)^{\wedge}(n)\right\}_{n \in \mathbb{N}_0}$, $J \in \mathbb{Z}$, is called the generating symbol of an $\mathcal{H}$-scaling function. The corresponding family $\left\{\Phi_J\right\}_{J \in \mathbb{Z}}$ of kernel functions given by

$$\Phi_J(x,y) = \sum_{n=0}^{\infty} \left(\Phi_J\right)^{\wedge}(n) U_n^*(x) U_n^*(y), \quad x, y \in \Sigma, \tag{9}$$

is called $\mathcal{H}$-scaling function. In order to define the associated $\mathcal{H}$-wavelets we let $\left\{\left(\Phi_J\right)^{\wedge}(n)\right\}_{n \in \mathbb{N}_0}$, $J \in \mathbb{Z}$, be the generating symbol of an $\mathcal{H}$-scaling function. Then the generating symbol $\left\{\left(\Psi_J\right)^{\wedge}(n)\right\}_{n \in \mathbb{N}_0}$, $J \in \mathbb{Z}$, of the associated $\mathcal{H}$-wavelet is defined by the refinement equation

$$\left(\Psi_J\right)^{\wedge}(n) = \left(\Phi_{J+1}\right)^{\wedge}(n) - \left(\Phi_J\right)^{\wedge}(n), \quad n \in \mathbb{N}_0. \tag{10}$$

The family $\left\{\Psi_J\right\}_{J \in \mathbb{Z}}$ of $\mathcal{H}$-product kernels given by $\Psi_J(x,y) = = \sum_{n=0}^{\infty} \left(\Psi_J\right)^{\wedge}(n) U_n^*(x) U_n^*(y)$, $x, y \in \Sigma$, is called $\mathcal{H}$-wavelet associated to the $\mathcal{H}$-scaling function $\left\{\Phi_J\right\}_{J \in \mathbb{Z}}$. The corresponding mother wavelet is denoted by Ψ_0. By virtue of the scaling functions and wavelets we define the scale spaces $\mathcal{V}_J$ and the detail spaces $\mathcal{W}_J$ by

$$\mathcal{V}_J = \left\{\Phi_J * F \middle| F \in \mathcal{H}\right\} \quad \text{and} \quad \mathcal{W}_J = \left\{\Psi_J * F \middle| F \in \mathcal{H}\right\}. \tag{11}$$

The spaces $\mathcal{V}_J$ represent the scale approximation of F at scale J and the corresponding operator $T_J(F) = \Phi_J * F$ can be interpreted as a low pass filter, whereas the spaces $\mathcal{W}_J$ represent the wavelet approximation of F at scale J and the corresponding operator $R_J(F) = \Psi_J * F$ can be interpreted as a band pass filter. We have the decomposition $\mathcal{V}_{J+1} = \mathcal{V}_J + \mathcal{W}_J$ and the limit relation (in $\mathcal{H}$-sense) $\lim_{J \to \infty} \Phi_J * F = F$ which leads to the multiresolution analysis given by the nested sequence of scale spaces

$$\ldots \subset \mathcal{V}_J \subset \mathcal{V}_{J+1} \subset \ldots \subset \mathcal{H}, \tag{12}$$

and

$$\mathcal{H} = \overline{\bigcup_{J=-\infty}^{\infty} \mathcal{V}_J}^{\|\cdot\|_{\mathcal{H}}} . \tag{13}$$

Therefore, we can decompose the space $\mathcal{V}_J$ for each scale $J \in \mathbb{Z}$ in one 'basic' scale space and several detail spaces: $\mathcal{V}_J = \mathcal{V}_{J_0} + \sum_{j=J_0}^{J-1} \mathcal{W}_j$.

In the following subsection we will remind the Hilbert spaces $\mathcal{L}^2\left([-1,1]\right)$ used for Legendre wavelets and $\mathcal{L}^2(\Omega)$ used for spherical wavelets which are of importance for the time–space decomposition.

3.1. Wavelets for the Time and Space Domain

Legendre Wavelets

We consider $\mathcal{H} = \mathcal{L}^2\left([-1,1]\right)$, the space of square-integrable functions $F:[-1,1] \to \mathbb{R}$, i.e., we let $\Sigma = [-1,1]$. This choice leads to the so-called Legendre wavelets, cf. *Beth and Viell (1998)*. We already defined the inner product $(F,G)_{\mathcal{L}^2([-1,1])}$ and the orthonormal system of Legendre polynomials P_n^*. The $\mathcal{L}^2\left([-1,1]\right)$-admissible product kernels then are given by

$$\Gamma(s,t) = \sum_{n=0}^{\infty} \Gamma^{\wedge}(n) P_n^*(s) P_n^*(t), \quad s,t \in [-1,1], \tag{14}$$

and the convolution of Γ against F is given by

$$(\Gamma * F)(t) = \sum_{n=0}^{\infty} \Gamma^{\wedge}(n) F^{\wedge}(n) P_n^*(t), \quad t \in [-1,1]. \tag{15}$$

Spherical Wavelets

In case of the scalar spherical wavelet theory we let $\Sigma = \Omega$ and consider $\mathcal{H} = \mathcal{L}^2(\Omega)$. As an $\mathcal{L}^2(\Omega)$-orthonormal system we choose the system $\{Y_{n,k}\}_{n \in \mathbb{N}_0,\, k=1,\ldots,2n+1}$ of spherical harmonics of degree n and order k. The $\mathcal{L}^2(\Omega)$-product kernels have the following representation

$$\Gamma(\xi,\eta) = \sum_{n=0}^{\infty} \sum_{k=1}^{2n+1} \Gamma^{\wedge}(n) Y_{n,k}(\xi) Y_{n,k}(\eta), \quad \xi,\eta \in \Omega, \tag{16}$$

and the convolution of Γ against F is given by

$$(\Gamma * F)(\xi) = \sum_{n=0}^{\infty} \sum_{k=1}^{2n+1} \Gamma^{\wedge}(n) F^{\wedge}(n,k) Y_{n,k}(\xi), \qquad \xi \in \Omega. \tag{17}$$

4. TIME-SPACE MULTIRESOLUTION ANALYSIS

We will now combine the Legendre wavelet expansion for the temporal analysis with the spherical wavelet expansion for the analysis of spatial variations. This is performed by introducing time-space dependent tensor product wavelets as done in *Freeden (1999)*, *Maier (2002)*, *Michel (1999)*. In contrast to the approaches described there we adapt the idea of the two-dimensional multiresolution in $\mathcal{L}^2(\mathbb{R}^2)$ given in *Louis et al. (1998)*. We arrive at one single scale in time and space and, therefore, get a time–space multiresolution. Starting point of our considerations is the space $\mathcal{L}^2([-1,1]\times\Omega)$ where without loss of generality we assume the time interval to be normalized to the interval $[-1,1]$. The scalar product of $F, G \in \mathcal{L}^2([-1,1]\times\Omega)$ is given by

$$(F,G)_{\mathcal{L}^2([-1,1]\times\Omega)} = \int_{-1}^{1} \int_{\Omega} F(t;\xi) G(t;\xi)\, d\omega(\xi)\, \mathrm{d}t. \tag{18}$$

We assume that the time dependency is fully described by the spatial Fourier coefficients, i.e.,

$$F(t;\xi) = \sum_{n=0}^{\infty} \sum_{k=1}^{2n+1} F^{\wedge}(n,k)(t) Y_{n,k}(\xi), \tag{19}$$

with

$$F^{\wedge}(n,k)(t) = \sum_{n'=0}^{\infty} F^{\wedge}(n';n,k) P_{n'}^{*}(t). \tag{20}$$

Note that for notational reasons in the following n' will always be used in case of time, whereas n will be used in space. We finally arrive at

$$F = \sum_{n'=0}^{\infty} \sum_{n=0}^{\infty} \sum_{k=1}^{2n+1} F^{\wedge}(n';n,k) P_{n'}^{*} Y_{n,k} \tag{21}$$

in $\mathcal{L}^2([-1,1]\times\Omega)$-sense.

Our aim is to define the scaling functions and wavelets in such a way that we result in a multiresolution of $\mathcal{L}^2([-1,1]\times\Omega)$ of the form

$$\ldots \subset \tilde{\mathcal{V}}_J \subset \tilde{\mathcal{V}}_{J+1} \subset \ldots \subset \mathcal{L}^2([-1,1]\times\Omega) \tag{22}$$

and

$$\mathcal{L}^2\left([-1,1]\times\Omega\right)=\overline{\bigcup_{J=-\infty}^{\infty}\tilde{\mathcal{V}}_J}^{\|\cdot\|_{\mathcal{L}^2([-1,1]\times\Omega)}}. \tag{23}$$

We start with the definition of the generating symbol of time–space scaling functions. Let $\left\{\left(\Phi'_J\right)^{\wedge}\left(n'\right)\right\}_{n'\in\mathbb{N}_0}$, $J\in\mathbb{Z}$, be the generating symbol of a temporal scaling function and let $\left\{\left(\Phi_J\right)^{\wedge}\left(n\right)\right\}_{n\in\mathbb{N}_0}$, $J\in\mathbb{Z}$, be the generating symbol of a spatial scaling function. Then the generating symbol of the time-space (tensor product) scaling function is given by the sequence $\left\{\left(\tilde{\Phi}_J\right)^{\wedge}\left(n';n\right)\right\}_{n',\,n\in\mathbb{N}_0}$, with

$$\left(\tilde{\Phi}_J\right)^{\wedge}\left(n';n\right)=\left(\Phi'_J\right)^{\wedge}\left(n'\right)\left(\Phi_J\right)^{\wedge}\left(n\right). \tag{24}$$

The family of kernel functions $\left\{\tilde{\Phi}_J\right\}_{J\in\mathbb{Z}}$ defined by

$$\tilde{\Phi}_J\left(s,t;\xi,\eta\right)=\sum_{n'=0}^{\infty}\sum_{n=0}^{\infty}\sum_{k=1}^{2n+1}\left(\tilde{\Phi}_J\right)^{\wedge}\left(n';n\right)P^*_{n'}\left(s\right)P^*_{n'}\left(t\right)Y_{n,k}\left(\xi\right)Y_{n,k}\left(\eta\right), \tag{25}$$

where $s,t\in[-1,1]$ and $\xi,\eta\in\Omega$, denotes the time-space (tensor product) scaling functions. Since we have two refinement equations

$$\left(\Psi'_J\right)^{\wedge}\left(n'\right)=\left(\Phi'_{J+1}\right)^{\wedge}\left(n'\right)-\left(\Phi'_J\right)^{\wedge}\left(n'\right), \tag{26a}$$

$$\left(\Psi_J\right)^{\wedge}\left(n\right)=\left(\Phi_{J+1}\right)^{\wedge}\left(n\right)-\left(\Phi_J\right)^{\wedge}\left(n\right), \tag{26b}$$

which have to be fulfilled simultaneously we get

$$\begin{aligned}\left(\Phi'_{J+1}\right)^{\wedge}\left(n'\right)\left(\Phi_{J+1}\right)^{\wedge}\left(n\right)&=\left(\Phi'_J\right)^{\wedge}\left(n'\right)\left(\Phi_J\right)^{\wedge}\left(n\right)+\left(\Psi'_J\right)^{\wedge}\left(n'\right)\left(\Phi_J\right)^{\wedge}\left(n\right)\\&+\left(\Phi'_J\right)^{\wedge}\left(n'\right)\left(\Psi_J\right)^{\wedge}\left(n\right)+\left(\Psi'_J\right)^{\wedge}\left(n'\right)\left(\Psi_J\right)^{\wedge}\left(n\right).\end{aligned} \tag{27}$$

This leads to the definition of two hybrid wavelets $\tilde{\Psi}^1_J$ and $\tilde{\Psi}^2_J$ and one pure wavelet $\tilde{\Psi}^3_J$:

$$\begin{aligned}\tilde{\Psi}^i_J\left(s,t;\xi,\eta\right)=\sum_{n'=0}^{\infty}\sum_{n=0}^{\infty}\sum_{k=1}^{2n+1}\left(\tilde{\Psi}^i_J\right)^{\wedge}\left(n';n\right)P^*_{n'}\left(s\right)P^*_{n'}\left(t\right)Y_{n,k}\left(\xi\right)Y_{n,k}\left(\eta\right),\\ i\in\{1,2,3\},\end{aligned} \tag{28}$$

with the symbols

$$\left(\tilde{\Psi}_J^1\right)^{\wedge}(n';n)=\left(\Phi'_J\right)^{\wedge}(n')\left(\Psi_J\right)^{\wedge}(n), \tag{29a}$$

$$\left(\tilde{\Psi}_J^2\right)^{\wedge}(n';n)=\left(\Psi'_J\right)^{\wedge}(n')\left(\Phi_J\right)^{\wedge}(n), \tag{29b}$$

$$\left(\tilde{\Psi}_J^3\right)^{\wedge}(n';n)=\left(\Psi'_J\right)^{\wedge}(n')\left(\Psi_J\right)^{\wedge}(n). \tag{29c}$$

For deducing the multiresolution we first introduce the time-space convolution. Let $F\in\mathcal{L}^2\left(\left[-1,1\right]\times\Omega\right)$ and let Γ be a kernel function of the form

$$\Gamma(s,t;\xi,\eta)=\sum_{n'=0}^{\infty}\sum_{n=0}^{\infty}\sum_{k=1}^{2n+1}\Gamma^{\wedge}(n';n)P_{n'}^{*}(s)P_{n'}^{*}(t)Y_{n,k}(\xi)Y_{n,k}(\eta). \tag{30}$$

The time-space convolution of Γ against F is defined by

$$\begin{aligned}(\Gamma * F)(t;\eta)&=\int_{-1}^{1}\int_{\Omega}\Gamma(s,t;\xi,\eta)F(s;\xi)\,d\omega(\xi)\,\mathrm{d}s\\&=\sum_{n'=0}^{\infty}\sum_{n=0}^{\infty}\sum_{k=1}^{2n+1}\Gamma^{\wedge}(n';n)F^{\wedge}(n';n,k)P_{n'}^{*}(t)Y_{n,k}(\eta).\end{aligned} \tag{31}$$

Now we introduce the scale and detail spaces. Let $\left\{\tilde{\Phi}_J\right\}$ be the time-space scaling functions and let $\left\{\tilde{\Psi}_J^1\right\}$, $\left\{\tilde{\Psi}_J^2\right\}$ and $\left\{\tilde{\Psi}_J^3\right\}$ be the associated hybrid and pure time-space wavelets at scale J. Then the pure time-space scale spaces are defined by

$$\tilde{\mathcal{V}}_J=\left\{\tilde{\Phi}_J * F\,\middle|\,F\in\mathcal{L}^2\left(\left[-1,1\right]\times\Omega\right)\right\}. \tag{32}$$

The hybrid and pure time-space detail spaces are given by

$$\tilde{\mathcal{W}}_J^i=\left\{\tilde{\Psi}_J^i * F\,\middle|\,F\in\mathcal{L}^2\left(\left[-1,1\right]\times\Omega\right)\right\},\qquad i\in\{1,2,3\}. \tag{33}$$

The next theorem which shows that the characteristics of a multiresolution analysis are fulfilled by the scale and detail spaces can be proven similar to *Maier (2002)*.

Theorem 4.1. For $J\in\mathbb{Z}$ let $\left\{\tilde{\Phi}_J\right\}$ be time-space scaling functions and let $\left\{\tilde{\Psi}_J^1\right\}$, $\left\{\tilde{\Psi}_J^2\right\}$ and $\left\{\tilde{\Psi}_J^3\right\}$ be the associated hybrid and pure time-space wavelets. Suppose that $F\in\mathcal{L}^2\left(\left[-1,1\right]\times\Omega\right)$. Then

$$F=\lim_{J\to\infty}\left(\tilde{\Phi}_J * F\right)=\lim_{J\to\infty}\left(\tilde{\Phi}_{J_0} * F+\sum_{j=J_0}^{J}\sum_{i=1}^{3}\tilde{\Psi}^i{}_j * F\right) \tag{34}$$

holds true in the sense of the $\mathcal{L}^2\left(\left[-1,1\right]\times\Omega\right)$-metric. Accordingly for the time-space scale spaces and detail spaces we have

$$\tilde{\mathcal{V}}_J = \tilde{\mathcal{V}}_{J_0} + \sum_{j=J_0}^{J-1}\sum_{i=1}^{3}\tilde{\mathcal{W}}_j^i \tag{35}$$

with $J, J_0 \in \mathbb{Z}$ and $J_0 \le J$.

5. NUMERICAL RESULTS WITH SYNTHETIC AND REAL DATA

This section is dedicated to the numerical computations with synthetic and real data as application of the time-space multiresolution method explained in the last section. First we present some results based on synthetically generated data in order to demonstrate the efficiency of this method. Then some results for real Earth's gravitational data from the satellite mission GRACE and hydrological data (WGHM) are given. These data have been provided from our project partners from GeoForschungsZentrum (GFZ) Potsdam, Department 1: Geodäsie und Fernerkundung within the TIVAGAM-project which is part of the Geotechnologies Special Programme funded by the Federal Ministry of Education and Research.

In case of the Earth's gravity field (GRACE) the data are given as a time series of 47 monthly data sets given from February 2003 to December 2006. The wavelet analysis requires equidistant data in time and for reasons of two missing months (June 2003 and January 2004) we have to complete the time series. For simplicity we use linear interpolation because this does not really influence the results. The monthly data sets for the gravity field are given as spherical harmonic expansions complete up to degree and order 55. In case of hydrological data (WGHM) we also use 47 monthly data sets from February 2003 to December 2006 which are given as spherical harmonic coefficients up to degree and order 55.

For abbreviation we restrict our numerical realization on the so-called cubic polynomial wavelet. The symbol $\left(\tilde{\Phi}_J\right)^{\wedge}\left(n';n\right)$ of the corresponding scaling functions in time and space (Eq.(25)) is composed by the temporal and spatial symbols $\left(\Phi'_J\right)^{\wedge}\left(n\right)$ and $\left(\Phi_J\right)^{\wedge}\left(n\right)$ given by

$$\left(\Phi'_J\right)^{\wedge}\left(n\right) = \left(\Phi_J\right)^{\wedge}\left(n\right) = \begin{cases} \left(1-2^{-J}n\right)^2\left(1+2^{1-J}n\right) & , \quad 0 \le n < 2^J \\ 0 & , \quad n \ge 2^J \end{cases} \tag{36}$$

for $n, J \in \mathbb{N}_0$. Note that for the computations the scale J is non-negative. Fig. 1 and Fig. 2 show the wavelet symbols and the wavelet functions, respectively, where the wavelet symbols (both in time and space) are calculated via the refinement Eq.(10).

Phenomena which occur both in time and space have to be described using four dimensions, one in time and three in space, which leads to difficulties as far as the presentation of the results is concerned. To extract the important characteristics we

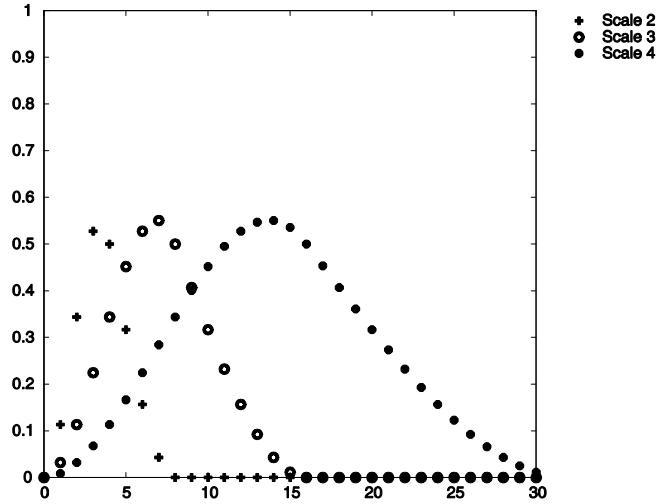

Fig. 1. Wavelet symbols $n \mapsto \left(\Psi_J\right)^{\wedge}\left(n\right)$ for $n = 0, 1, \ldots, 30$ and $J = 2, 3, 4$ for the cubic polynomial wavelet.

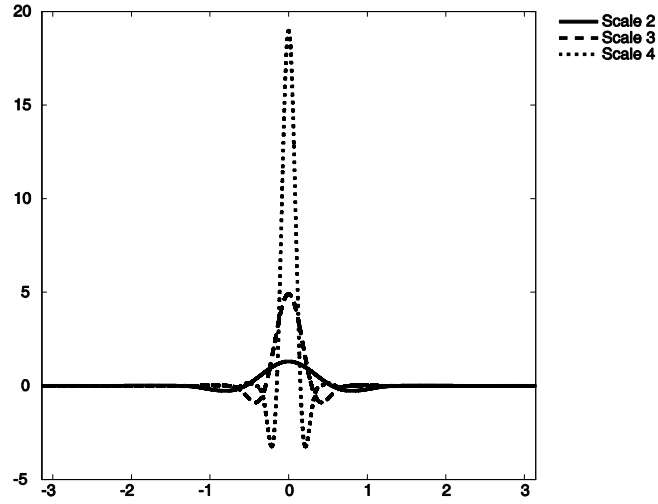

Fig. 2. Wavelet functions $\vartheta \mapsto \Psi_J\left(\cos\vartheta\right)$ for $\vartheta \in \left[-\pi, \pi\right]$ and $J = 2, 3, 4$ for the cubic polynomial wavelet.

decided to use two types of presentation: In order to show the spatial distribution of the detected phenomena we plot the maximum of the absolute values of the scale or detail parts over the whole time interval at each position. Thereby, we get an idea where the positions of great or moderate changes are situated. Furthermore we select special positions located in regions of interest and plot the time dependent courses. This helps us to visualize seasonal or other temporal variations.

For reasons of comparison between different scales in case of detail parts we have adapted the color scale of the corresponding plots. The values 'min' and 'max' under these figures give us information about the real minimal and maximal values. Note that for the computations the time interval has to be normalized to [−1, 1], but for reasons of understanding we prefer the original marks of the dates in the plots.

5.1. Synthetically Generated Data

In order to get a realistic simulation of the situation given in case of real GRACE data we decided to analyze a synthetically generated time series consisting of 40 dates. Starting from a trial function $F(t;\xi)$, $t \in [1,40]$, $\xi \in \Omega$, we calculate the corresponding spherical harmonic coefficients $F^{\wedge}(n,k)(t)$, $n \in \mathbb{N}_0$, $k = 1, \ldots, 2n+1$, $t \in [1,40]$, to obtain the input data sets. In order to give an impression of the efficiency of the algorithm we use a trial function which contains temporal and spatial variations (a moving 'smoothed peak'). The trial function depends on time and space and is given by

$$F(t;\xi) = \begin{cases} \dfrac{1}{\left|\xi - \dfrac{29}{30}\eta(t)\right|} & , \quad \text{for all } t \in [10,30], \\ 0 & , \quad \text{for all } t \in [1,9] \cup [31,40], \end{cases} \tag{37}$$

where $\eta(t)$ moves along the equator. The maximum value, i.e. $v_{max} = 30$, of the first smoothed peak, i.e., for $t = 10$, is located at 0°N 90°W and the last one at 0°N 90°E, such that we have 21 points at intervals of 9°. The maximum values of the trial function over the whole time interval are plotted in Fig. 3a. The time dependent courses are given for four points: 0°N 0°E (1st point), 0°N 45°E (2nd point), 4.5°N 0°E (3rd point), 9°N 0°E (4th point) (see Fig. 3b). Consequently, in this synthetic example we have a covering of two high-frequency phenomena: First, the 21 smoothed peaks described in the text above and, secondly, two jumps of lower size arising from the fact that the peaks are only set from date 10 to date 30.

Results of these synthetically generated data demonstrate the 'zooming-in' effect of the multiscale analysis, i.e., with increasing scale finer and finer structures are detected. Thus, our synthetic smoothed peaks represent detail information which we expect to find out in higher scales. In case of the first hybrid detail parts, i.e. $\tilde{\Psi}_j^1 * F$ in Eq.(3), shown in the left column of Fig. 4, the 'zooming-in' effect is clearly seen. Scale 4 (Fig. 4a) filters out the coarser structures whereas in scale 6 (Fig. 4e) a sufficiently good space localization is achieved. These results can also be seen in the time dependent courses of the second hybrid detail parts, i.e. $\tilde{\Psi}_j^2 * F$, shown in the right column of Fig. 4. Moreover

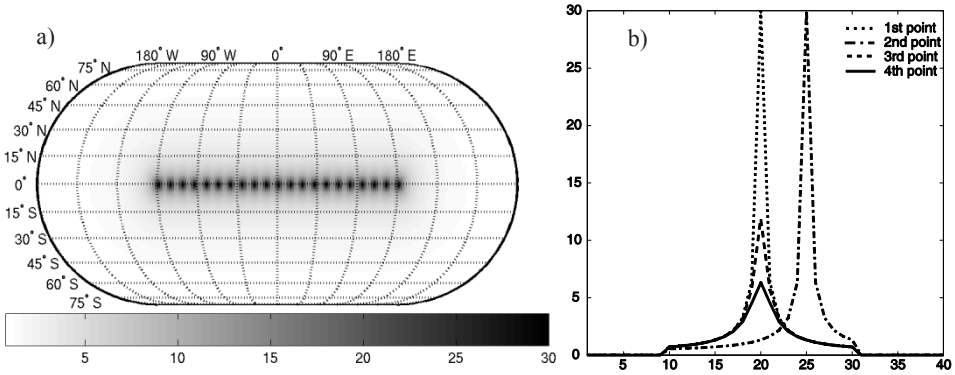

Fig. 3. Time and space dependent trial function for a moving smoothed peak as described in Eq.(37). **a)** Maximum of the absolute values of the trial function described in Section 5.1., **b)** Time dependent courses of the trial function of the four different points given in Section 5.1.

the decreasing influence of the different smoothed peaks moving in Northern direction (3rd and 4th point) can be well realized. The small jumps at date 10 and 30 are also detected in case of these second hybrid parts but in case of the pure detail parts this phenomena is hided by the smoothed peaks. For this reason in Section 5.2 we concentrate on the hybrid detail parts which show a better separation in time and space.

5.2. Earth's Gravitational Data (GRACE)

In Section 5.1 about synthetically generated data we demonstrated in which way the algorithm filters out certain variations in time and space on the basis of easily structured input data. Now, our aim is to present which temporal and spatial phenomena are found out from real input data and, therefore, we present some results based on Earth's gravitational data sets from the satellite mission GRACE. In this paper we concentrate on showing that the method works on real data but we do not aim at interpreting these results with respect to geophysical phenomena. The data are given as monthly data sets for the time interval from February 2003 till December 2006.

As stated in Theorem 4.1 the method is based on a (time-space) multiresolution analysis. Fig. 5 illustrates the increasing reconstruction of the original signal with higher scale J. Turning from scale 4 to scale 5 three detail parts $\tilde{\mathcal{W}}_4^i$, $i \in \{1,2,3\}$ are added to $\tilde{\mathcal{V}}_4$ in order to reach the reconstruction $\tilde{\mathcal{V}}_5$ of the next scale. In the following we analyze the detail parts $\tilde{\mathcal{W}}_J^1$ and $\tilde{\mathcal{W}}_J^2$ of the multiresolution of the GRACE data. Because of the results obtained in Section 5.1, where we have described that some detail information may not be filtered out using the pure details, we show the changes in the spatial dimension using the first hybrid detail parts whereas temporal variations are filtered out best by the second hybrid detail parts.

Figs. 6 and 7 show the results for the first and second hybrid detail parts based on the GRACE data. In Fig. 6a only coarse, low-frequency structures can be recongnized whereas with increasing scale (Fig. 6b–d) more and more high-frequency information is visible. Due to the fact that the data are just given up to degree and order 55, results with scales higher than 6 in case of the cubic polynomial wavelet cannot be interpreted. The existence of stripes oriented North to South in Fig. 6d indicates errors in high-frequency components (see *Swenson and Wahr, 2006*).

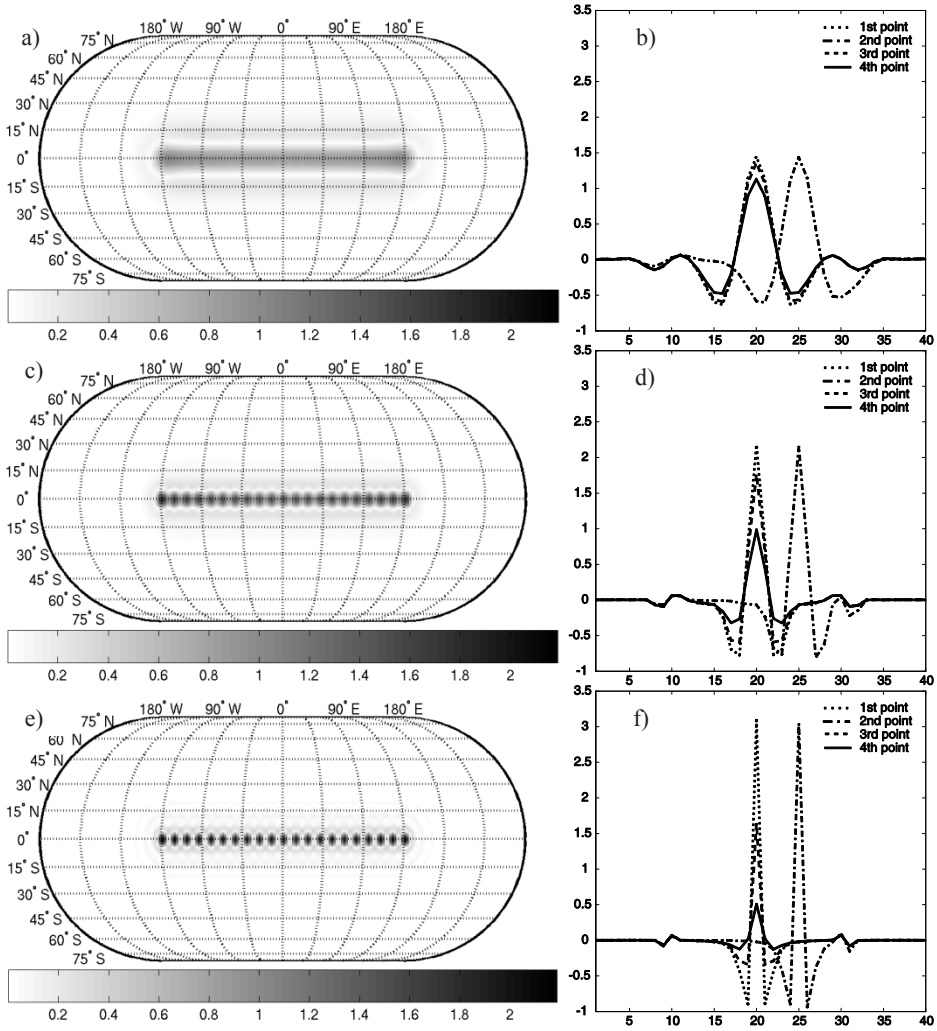

Fig. 4. Maximum of the absolute values of the first hybrid detail parts (left column) and time dependent courses of the corresponding second hybrid detail parts (right column) calculated with cubic polynomial wavelet in time and space at different scales based on the data described in Section 5.1. **a-b)** Scale 4 (*min* = 0.0007, *max* = 1.0294), **c-d)** Scale 5 (*min* = 0.0002, *max* = 1.8409), **e-f)** Scale 6 (*min* = 0.0025, *max* = 2.1865).

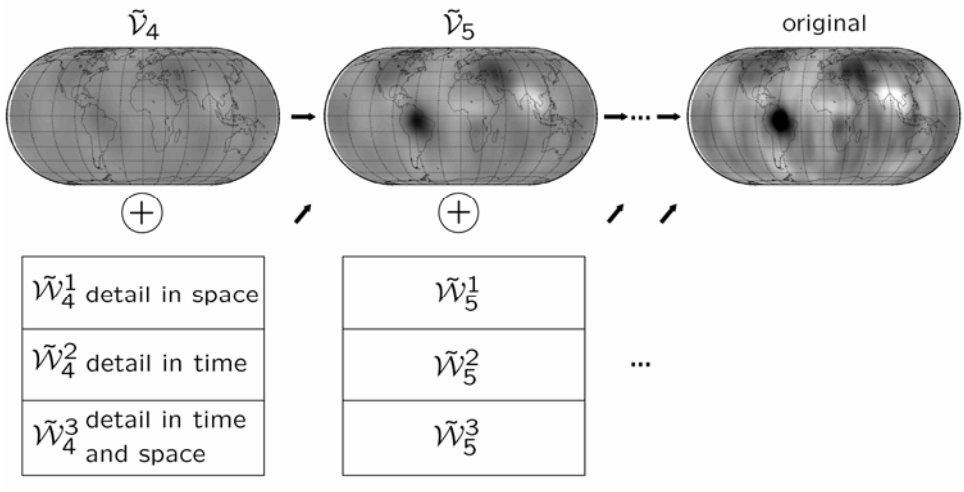

Fig. 5. Demonstration of a multiresolution.

For the visualization of the time dependent course we choose exemplarily three different cities, i.e., three different locations in the space domain. We select one point on the Southern hemisphere (Manaus) and two points on the Northern hemisphere (Dacca and Kaiserslautern). Kaiserslautern is located within a region of moderate seasonal variations in the water balance, whereas the other two cities show the time dependent course in well–known regions of great changes (Amazonas basin and Ganges basin). In Fig. 7 the time dependent courses of the second hybrid detail parts of these three cities are plotted. The seasonal variations can be seen best in scales 3 and 4. Even for Kaiserslautern which is located in a region with moderate variations the course of the values demonstrates the seasonal course.

5.3. Comparison of GRACE Data with the Hydrological Model WGHM

The preprocessed GRACE data used for the computations in Section 5.2 mainly reflects continental water storage variations which show regional differences. This is the reason why we apply the time space multiresolution for the comparison of the satellite GRACE data with the hydrological model WGHM. The results for the calculations with the WGHM data are quite similar to those of the GRACE data as expected. Therefore, we do not go into the details but we compute the scale depending local and global correlation coefficients of both data sets.

As well as the GRACE data the hydrological data are available as a time series of spherical harmonics coefficients up to degree and order 55. The time series consists of 47 monthly data sets (from February 2003 till December 2006).

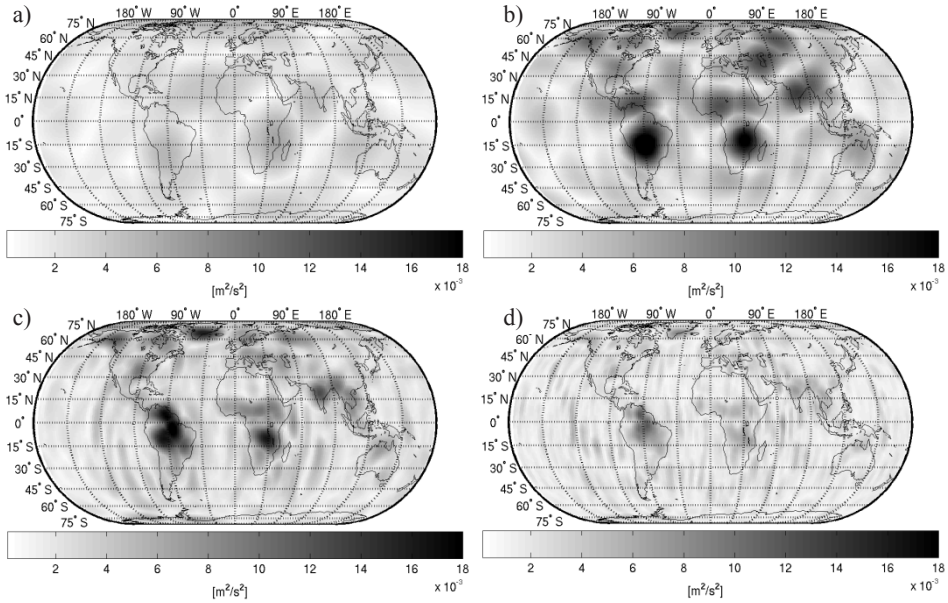

Fig. 6. Maximum of the absolute values of the first hybrid detail parts calculated with cubic polynomial wavelet in time and space at different scales based on a time series of 47 monthly data sets (from February 2003 till December 2006, in 10^{-3} m^2/s^2). **a)** Scale 2 (*min* = 0.0001, *max* = 0.0065), **b)** Scale 3 (*min* = 0.0002, *max* = 0.0222), **c)** Scale 4 (*min* = 0.0004, *max* = 0.0190), **d)** Scale 5 (*min* = 0.0004, *max* = 0.0118).

In Fig. 8 the local correlation coefficients on the continents and, additionally, the corresponding 'global' correlation coefficients (on the continents) are shown. Fig. 8a presents the local correlation coefficients computed from the original GRACE and WGHM data. Especially, in Asia, North Africa and North America we recognize regions with bad correlation between the preprocessed satellite data (GRACE) and the hydrological model (WGHM). With our method we are able to show how these local correlation coefficients are composed with respect to different scales. We decided to consider the correlation coefficients from the pure detail parts (see Fig. 8b–d) because they visualize the correlation of the data analyzed both in time and space. Obviously, there exist some regions which also for higher scales have an above-average good correlation, i.e. in these regions the GRACE and WGHM data locally coincide much better (Mississippi, Amazonas, Ganges). Although the 'global' correlation coefficients get worse with increasing scale, these regions with locally good correlation are clearly visualized.

6. CONCLUSIONS

The aim of this paper is to demonstrate the effectiveness of the time-space multiscale analysis using tensor product wavelets. We apply the algorithm on data sets for the gravitational potential given as spherical harmonic coefficients. Starting from the theory

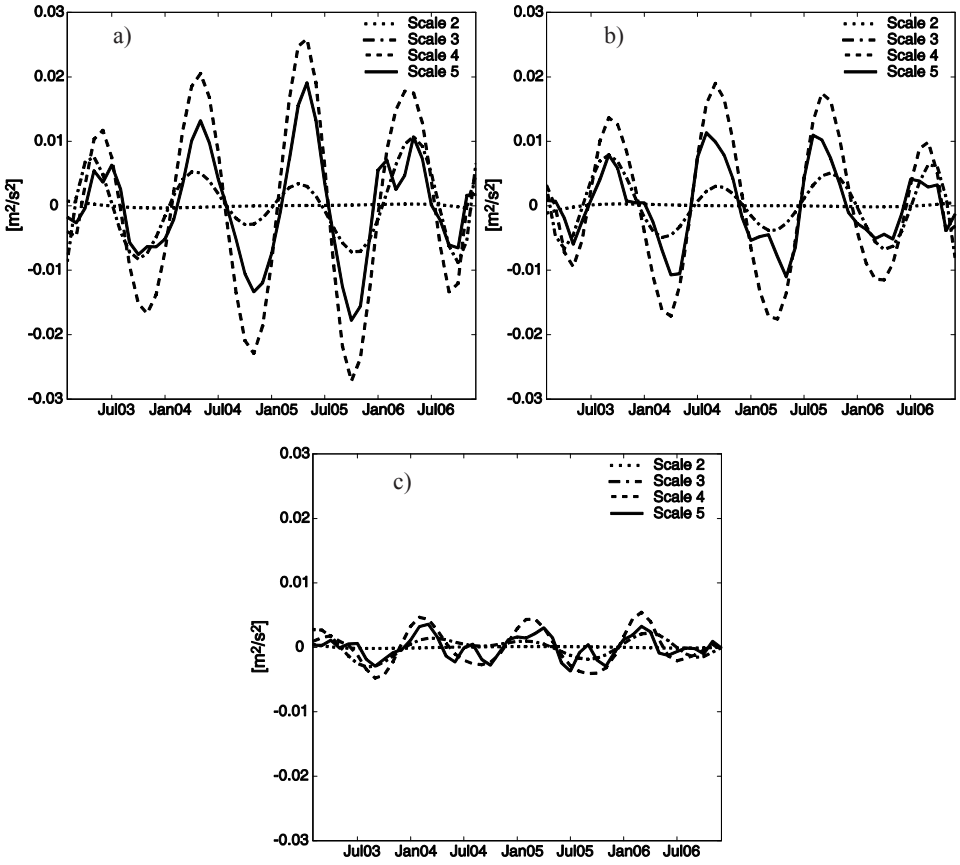

Fig. 7. Time dependent courses of the second hybrid detail parts calculated with cubic polynomial wavelet in time and space at different scales based on a time series of 47 monthly data sets (from February 2003 till December 2006). **a)** Manaus (3°S, 60°W), **b)** Dacca (23°N, 90°E), **c)** Kaiserslautern (49°N, 7°E).

of spherical wavelets introduced by the Geomathematics Group of TU Kaiserslautern tensor product wavelets are built up using the Legendre wavelets in time. This leads to a unified setup of multiresolution in the time-space domain because one single scale for both time and space suffices. As known from classical multidimensional multiscale analysis we decompose the signal into one smoothed part and three detail parts. These detail components are filtered out by use of one pure wavelet and two hybrid wavelets. The algorithm is demonstrated both by means of a synthetically generated example and real data sets. The zooming-in property with increasing scale is clearly shown in time as well as in space. Moreover, with the help of the time-space multiresolution method we are able to compare two time series locally both in time and space using correlation coefficients. Summing up the time-space multiscale analysis is an efficient algorithm to extract all at once temporally and spatially local phenomena.

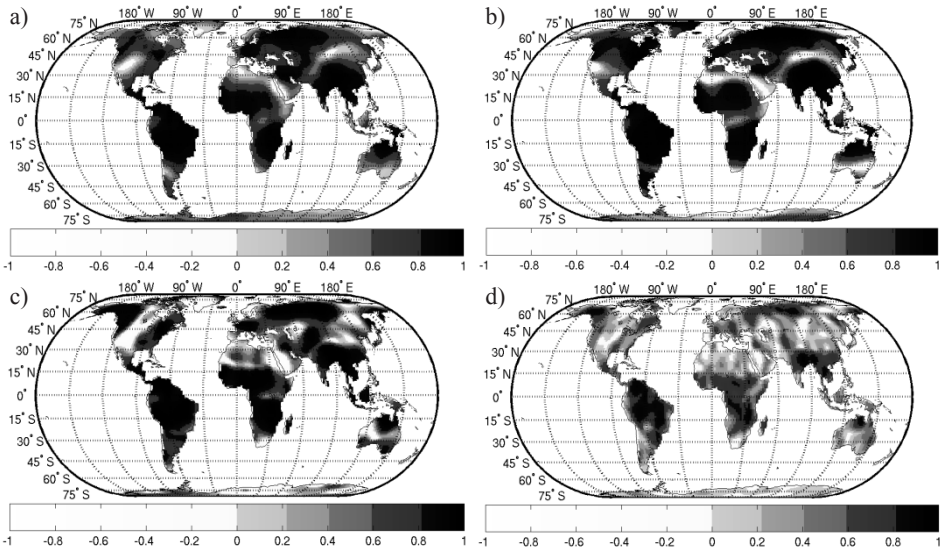

Fig. 8. Local correlation coefficients (*Lcc*) between GRACE and WGHM and in brackets the corresponding global correlation coefficients c_{gl}. **a)** *Lcc* of the original data ($c_{gl} = 0.77$), **b)** *Lcc* of the pure detail parts at scale 3 ($c_{gl} = 0.83$), **c)** *Lcc* of the pure detail parts at scale 4 ($c_{gl} = 0.80$), **d)** *Lcc* of the pure detail parts at scale 5 ($c_{gl} = 0.52$).

Acknowledgements: The authors gratefully acknowledge the support by the German Ministry of Education and Research (BMBF) and German Research Foundation (DFG) within the R&D-Programme Geotechnologies Special Programme "Observation System Earth from Space", 03F0424D, (publication number GEOTECH-317). We are also much obliged to GFZ Potsdam for providing us with all GRACE and WGHM data. Moreover we thank the members of the Geomathematics Group of TU Kaiserslautern for valuable discussions.

References

Beth S. and Viell M., 1998. Uni- und multivariate Legendre-Wavelets und ihre Anwendung zur Bestimmung des Brechungsindexgradienten. In: Freeden W. (Ed.), *Progress in Geodetic Science at GW 98*. Shaker Verlag, Aachen, Germany, 25–33.

Döll P., Kaspar F. and Lehner B., 2003. A global hydrological model for deriving water availability indicators: model tuning and validation. *J. Hydrol.*, **270**, 105–134.

Fengler M.J., Freeden W., Kohlhaas A., Michel V. and Peters T., 2007. Wavelet modelling of regional and temporal variations of the Earth's gravitational potential observed by GRACE. *J. Geodesy*, **81**, 5–15.

Freeden W., 1999. *Multiscale Modelling of Spaceborne Geodata*. Teubner, Stuttgart, Leipzig, Germany.

Freeden W. and Schneider F., 1998. An integrated wavelet concept of physical geodesy. *J. Geodesy*, **72**, 259–281.

Freeden W., Gervens T. and Schreiner M., 1998. *Constructive Approximation on the Sphere with Applications to Geomathematics*. Oxford Science Publications, Clarendon, U.K.

GRACE Mission. http://www.csr.utexas.edu/grace/.

Louis A.K., Maaß P. and Rieder A., 1998. *Wavelets: Theorie und Anwendungen*. Teubner, Stuttgart, Germany (in German).

Maaß P. and Stark H.-G., 1994. Wavelets and digital image processing. *Surveys on Mathematics in Industry*, **4**, 195–235.

Maier T., 2002. *Multiscale Geomagnetic Field Modelling from Satellite Data: Theoretical Aspects and Numerical Applications*. Ph.D. Thesis. Geomathematics Group, Department of Mathematics, University of Kaiserslautern, Kaiserslautern, Germany.

Michel V., 1999. *A Multiscale Method for the Gravimetry Problem - Theoretical and Numerical Aspects of Harmonic and Anharmonic Modelling*. Ph.D. Thesis. Geomathematics Group, Department of Mathematics, University of Kaiserslautern, Shaker Verlag, Aachen, Germany.

Müller C., 1966. *Spherical Harmonics, Vol.17*. Springer-Verlag, Berlin, Heidelberg, New York.

Swenson S. and Wahr J., 2006. Post-processing removal of correlated errors in GRACE data. *Geophys. Res. Lett.*, **33**, L08402, doi: 10.1029/2005GL025285.

Tapley B.D., Bettadpur S., Watkins M.M. and Reigber C., 2004. The gravity recovery and climate experiment: mission overview and early results. *Geophys. Res. Lett.*, **31**, L09607, doi: 10.1029/2004GL019920.

Viell M., 1998. *Die Theorie der uni- und multivariaten Legendre-Wavelets und ihre Anwendung in der Refraktionsanalyse.* Diploma Thesis, Geomathematics Group, Department of Mathematics, University of Kaiserslautern, Kaiserslautern, Germany (in German).

Wahr J., Swenson S., Zlotnicki V. and Velicogna I., 2004. Time-variable gravity from GRACE: first results. *Geophys. Res. Lett.*, **31**, L11501, doi: 10.1029/2004GL019779.